**CSIRO** PUBLISHING

*Exploration Geophysics*, 2016, **47**, 85–99
http://dx.doi.org/10.1071/EG14093

# The distortion tensor of magnetotellurics: a tutorial on some properties

Frederick E. M. Lilley

Research School of Earth Sciences, Australian National University, Canberra, ACT 0200, Australia.
Email: ted.lilley@anu.edu.au

**Abstract.** A $2 \times 2$ matrix is introduced which relates the electric field at an observing site where geological distortion applies to the regional electric field, which is unaffected by the distortion. For the student of linear algebra this matrix provides a practical example with which to demonstrate the basic and important procedures of eigenvalue analysis and singular value decomposition.

The significance of the results can be visualised because the eigenvectors of such a telluric distortion matrix have a clear practical meaning, as do their eigenvalues. A Mohr diagram for the distortion matrix displays when real eigenvectors exist, and tells their magnitudes and directions.

The results of singular value decomposition (SVD) also have a clear practical meaning. These results too can be displayed on a Mohr diagram. Whereas real eigenvectors may or may not exist, SVD is always possible. The ratio of the two singular values of the matrix gives a condition number, useful to quantify distortion. Strong distortion causes the matrix to approach the condition known as 'singularity'. A closely-related anisotropy number may also be useful, as it tells when a $2 \times 2$ matrix has a negative determinant by then having a value greater than unity.

**Key words:** distortion, eigenanalysis, magnetotelluric, Mohr, SVD, telluric.

Received 29 September 2014, accepted 12 March 2015, published online 1 May 2015

## Introduction

Three important matrices arise in magnetotelluric (MT) studies. The first matrix describes the distortion of measured electric fields. The second matrix is based on the MT observations themselves, of both magnetic and electric fields. The third matrix is the 'phase tensor', and is derived from the second matrix by computation.

The present paper addresses the first matrix, which commonly describes the distortion of measured electric fields quite locally, at an observing site. The more simple circumstances of this distortion matrix, in tensor form, are examined to establish some basic points. These points, once understood, may be useful in understanding the more complicated second and third matrices.

This paper expands upon a poster 'The distortion matrix for the student of linear algebra' that was presented in July 2012 at the 21st Electromagnetic Induction Workshop, held in Darwin, Australia. Some material is also drawn from an earlier publication (Lilley, 2012), enlarging on discussion there and refining its presentation.

A present stage of increased MT activity in Australia may bring newcomers to the subject. This paper hopes to contribute to a sound understanding of some basic theory by those who will, perhaps inevitably, have observations from complicated field situations to address.

Modern data sets may comprise simultaneous magnetic and electric field observations over arrays of sites. Such data sets offer many possibilities for the refined study and use, and also the avoidance, of the distortion characteristics described in this paper.

## Notation for axes and their rotation

Horizontal directions north and east will be denoted by axes $OX$ and $OY$, with $OZ$ vertically downwards. When rotated clockwise by angle $\theta'$ as shown in Figure 1, the axes will be denoted $OX'$ and $OY'$.

A rotation matrix $\mathbf{R}(\theta)$ will be introduced,

$$\mathbf{R}(\theta) = \begin{bmatrix} \cos\theta & \sin\theta \\ -\sin\theta & \cos\theta \end{bmatrix} \quad (1)$$

and the transpose of $\mathbf{R}(\theta)$ will be denoted by $\mathbf{R}^{\mathbf{T}}(\theta)$. Sometimes $\mathbf{R}^{\mathbf{T}}(\theta)$ will be written as $\mathbf{R}(-\theta)$, to which it is equal. For compactness of text, a $2 \times 2$ matrix such as that for $\mathbf{R}(\theta)$ in Equation 1 will in places be written

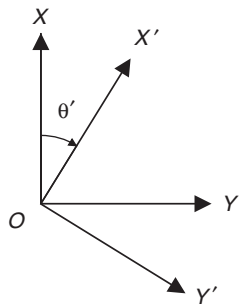


**Fig. 1.** The rotation of axes clockwise by angle $\theta'$, from $OX$ and $OY$ (north and east) to $OX'$ and $OY'$.

$$\mathbf{R}(\theta) = [\cos\theta, \sin\theta; -\sin\theta, \cos\theta] \quad (2)$$

Numerical examples will be used to illustrate points arising in this paper. For convenience, the values given will in places be rounded or truncated to four, three or two significant figures.

## The distortion tensor

The traditional method of telluric prospecting (Telford et al., 1976) relates the electric field $\mathbf{E^m}$ measured at a local site to the electric field $\mathbf{E^b}$ at a regional or base site by the distortion tensor $\boldsymbol{D}$ according to

$$\mathbf{E^m} = \boldsymbol{D}.\mathbf{E^b} \quad (3)$$

When matrix $\boldsymbol{D}$ is stated relative to axes $OX$, $OY$ (north and east), the values of its components relative to axes $OX'$, $OY'$ (which are rotated $\theta'$ clockwise from north and east as in Figure 1) will be those of a matrix $\boldsymbol{D}'$, given by

$$\begin{bmatrix} D'_{xx} & D'_{xy} \\ D'_{yx} & D'_{yy} \end{bmatrix} = \mathbf{R}(-\theta').\begin{bmatrix} D_{xx} & D_{xy} \\ D_{yx} & D_{yy} \end{bmatrix}.\mathbf{R}(\theta') \quad (4)$$

While generally $\boldsymbol{D}$ is frequency-dependent and complex, this paper takes the common model for the electric-field distortion of magnetotelluric observations for which $\boldsymbol{D}$ is in-phase (i.e. pure real, as for a direct current case) (Jones, 2012; Weidelt and Chave, 2012). Then for a change of electric field $\mathbf{E^b}$ at the regional site there will be, at the observing site, a change of electric field $\mathbf{E^m}$ generally of a different amplitude and generally in a different direction.

In the most simple case, the geological structure at the regional or base site will be one-dimensional (1D); that is, varying with depth only. The distortion of the regionally-induced electric field will be by a two-dimensional (2D) structure at the local site, and the distortion there will have 2D characteristics. The 2D axes of the distortion will then correspond to some geological property such as local strike, which it is valuable to determine. The knowledge of strike direction is of fundamental importance for interpretation and modelling.

Eigenanalysis and singular value decomposition (SVD) are two methods of linear algebra which it is natural to assess for applications to such studies (Eggers, 1982; LaTorraca et al., 1986; Yee and Paulson, 1987). If applied to the distortion tensor, as in this paper, eigenanalysis and SVD will individually determine, with a 90° ambiguity, the geologic strike direction for the most simple 2D case. In a more complicated case, the two methods individually may help to find a direction which is the strike of a 2D model approximating the actual situation. The methods will also show if a situation is far from 2D, so that 2D modelling may not be justified. Quantitative parameters for the 1D, 2D and 3D characteristics of a matrix are defined clearly.

This paper thus describes the application of eigenanalysis and SVD to the telluric distortion matrix. Telluric distortion may also be of wider interest to students of linear algebra who value a practical example which demonstrates these two methods. Both methods have great strength and wide application for large matrices. However examples of $2 \times 2$ matrices given to introduce eigenanalysis and SVD are sometimes artificial. The telluric distortion matrix provides a $2 \times 2$ example which is physically realistic, and which can be visualised.

When referring to matrices in this paper, the term 'observed point' will sometimes be used when plotting the number pair ($D_{xx}$, $D_{xy}$) on a diagram. The values of $D_{xx}$ and $D_{xy}$ are as in Equation 4. Though computed from field observations, they are 'observed' in the sense that they are relative to the axes of field observation, before any exercises of axis rotation are invoked.

## Eigenanalysis

Eigenvector analysis amounts to finding a direction of regional electric field change for which the measured local electric field change is in the same direction. The eigenvalue for that direction then gives the gain of the process, i.e. the amplitude of the local measured signal for unit amplitude regional signal. With reference to Equations 3 and 4 a direction is thus sought in which an $OX'$ regional signal is accompanied only by an $OX'$ local signal. This requirement can be regarded as finding an angle of axes rotation for which $D'_{yx}$ is zero, and leads to the solutions given in the section *Formal eigenvalue analysis* below. Commonly (but not always) there will be two real eigenvectors, each with an associated eigenvalue. For the example matrix

$$\boldsymbol{D} = \begin{bmatrix} 1.75 & 1.34 \\ 0.34 & 1.25 \end{bmatrix} \quad (5)$$

the eigenvector directions (19.3° and 144.2°) and the effects of the eigenvalues (2.22 and 0.78) are shown in Figure 2.

### *Formal eigenvalue analysis*

The eigenvalue problem (Strang, 2005) seeks solutions for the equation which expresses $\mathbf{E^m}$ and $\mathbf{E^b}$ to be parallel:

$$\mathbf{E^m} = \zeta\mathbf{E^b} \quad (6)$$

where $\zeta$ is a real scalar. Equation 6 may be combined with Equation 3 and cast as

$$(\boldsymbol{D} - \zeta\mathbf{I}).\mathbf{E^b} = \mathbf{0} \quad (7)$$

where $\mathbf{I}$ is the identity matrix [1, 0; 0,1]. For there to be a non-zero solution for $\mathbf{E^b}$, the determinant of $(\boldsymbol{D} - \zeta\mathbf{I})$ must be zero, and for the $2 \times 2$ distortion matrix, this condition gives what is known as the 'characteristic equation' for matrix $\boldsymbol{D}$:

$$\zeta^2 - (D_{xx} + D_{yy})\zeta + D_{xx}D_{yy} - D_{xy}D_{yx} = 0 \quad (8)$$

The characteristic equation is solved for the eigenvalues $\zeta_1$ and $\zeta_2$, and then eigenvectors are found corresponding to these eigenvalues.

The characteristic equation has solutions

$$\zeta_1, \zeta_2 = (D_{xx} + D_{yy})/2 \pm [(D_{xx} + D_{yy})^2 + 4(D_{xy}D_{yx} - D_{xx}D_{yy})]^{\frac{1}{2}}/2 \quad (9)$$

Three cases of Equation 9 are possible and of interest. Each will now be discussed separately.

### *Eigenvalues are real and different*

Taking as the first case the condition

$$(D_{xx} + D_{yy})^2 + 4(D_{xy}D_{yx} - D_{xx}D_{yy}) > 0 \quad (10)$$

the two roots of the characteristic equation are both real, different, and positive or negative depending on the signs and magnitudes of $(D_{xx} + D_{yy})$ and $(D_{xx}D_{yy} - D_{xy}D_{yx})$. These latter quantities are recognised as the trace (tr$\boldsymbol{D}$) and determinant (det$\boldsymbol{D}$) of $\boldsymbol{D}$.

The product of the two eigenvalues is given by

$$\zeta_1\zeta_2 = \det\boldsymbol{D} \quad (11)$$

and is positive if det$\boldsymbol{D}$ is positive, negative if det$\boldsymbol{D}$ is negative, and zero if det$\boldsymbol{D}$ is singular (in which case there will be an eigenvalue of zero).

In the case of the example matrix in Equation 5, this analysis gives the results displayed in Figure 2. The eigenvalues of 2.22

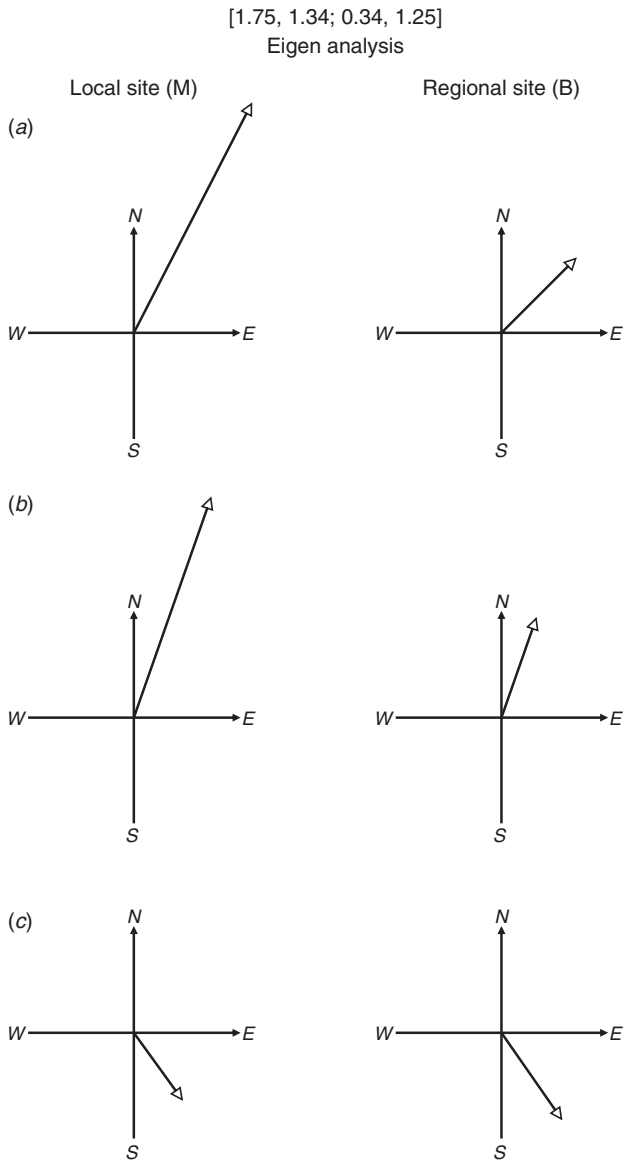


**Fig. 2.** Eigenvalue analysis. (*a*) For a general unit-amplitude signal (here at bearing 45°) at regional site B, the signal at local site M is not in the same direction and is not of unit amplitude. (*b*) For a unit-amplitude signal at B in the direction of an eigenvector (bearing 19.3°), the signal at M is in the same direction and is amplified by the eigenvalue (here 2.22). Note this eigenvector might equally well be drawn reversed at both sites B and M, in the direction of bearing 19.3° + 180° = 199.3°. (*c*) For a second unit-amplitude signal at B in the direction of a second eigenvector (bearing 144.2°), again the signal at M is parallel, and is amplified by the corresponding eigenvalue (an attenuation factor of 0.78 in this case). Note this second eigenvector might again equally well be drawn reversed at both sites B and M, in the direction of bearing 144.2° + 180° = 324.2°.

and 0.78 are given by Equation 9, and eigenvectors are found directly (for this 2 × 2 matrix) by expanding Equation 7 to give

$$(D_{xx} - \zeta_1)E_x^b + D_{xy}E_y^b = 0 \qquad (12)$$

which, for $D_{xx}$, $\zeta_1$ and $D_{xy}$ values of 1.75, 2.22 and 1.34 respectively, gives an $E_y^b/E_x^b$ ratio of 0.35, and so an eigenvector of bearing arctan(0.35), which is 19.3° (or 199.3°). Similarly, the $\zeta_2$ value of 0.78 gives an $E_y^b/E_x^b$ ratio of −0.72 and so an eigenvector of bearing arctan(−0.72), which is 144.2° (or 324.2°).

### *Eigenvalues are real and equal*

The second case occurs when

$$(D_{xx} + D_{yy})^2 + 4(D_{xy}D_{yx} - D_{xx}D_{yy}) = 0 \qquad (13)$$

The two roots of the characteristic equation are now both real (positive or negative), and equal. In fact,

$$\zeta_1 = \zeta_2 = (D_{xx} + D_{yy})/2 \qquad (14)$$

and the product of the two roots, $\zeta_1\zeta_2$, will always be positive. In this case there is only one direction for $\mathbf{E^m}$ and $\mathbf{E^b}$ to be parallel.

### *Eigenvalues are complex conjugate pairs*

The third case occurs when

$$(D_{xx} + D_{yy})^2 + 4(D_{xy}D_{yx} - D_{xx}D_{yy}) < 0 \qquad (15)$$

and the two roots of the characteristic equation form a complex conjugate pair. The product of the two roots, $\zeta_1\zeta_2$, will again always be positive. An equivalent way of expressing Inequality 15 is

$$(D_{xx} - D_{yy})^2 + 4D_{xy}D_{yx} < 0 \qquad (16)$$

In this third case there is no direction for which $\mathbf{E^m}$ and $\mathbf{E^b}$ are parallel.

### *Eigenvalues on Mohr diagrams*

Mohr diagrams may be used to display 2 × 2 matrices. Upon expanding Equation 4 for $D'_{xx}$, $D'_{xy}$, $D'_{yx}$ and $D'_{yy}$ it is seen that

$$D'_{xx} + D'_{yy} = D_{xx} + D_{yy} \qquad (17)$$

and

$$D'_{xy} - D'_{yx} = D_{xy} - D_{yx} \qquad (18)$$

Thus $(D'_{xx} + D'_{yy})$ and $(D'_{xy} - D'_{yx})$ are independent of $\theta'$ and are rotational invariants. Also it may be shown that

$$[D'_{xx} - (D_{xx} + D_{yy})/2]^2 + [D'_{xy} - (D_{xy} - D_{yx})/2]^2 = r^2 \qquad (19)$$

where

$$r^2 = [(D_{xy} + D_{yx})^2 + (D_{xx} - D_{yy})^2]/4 \qquad (20)$$

Equation 19 defines a circle when $D'_{xx}$ is plotted against $D'_{xy}$ as the axes are rotated and $\theta'$ varies. The centre of the circle is at the point $[(D_{xx} + D_{yy})/2, (D_{xy} - D_{yx})/2]$ and the circle is of radius $r$, another rotational invariant. On such a figure, axes for $D'_{yx}$ and $D'_{yy}$ may also be drawn, so that the variation with axis rotation of all components of $\boldsymbol{D}'$ is then displayed (Lilley, 1993). Other circles are also possible, for example if $D'_{yy}$ is plotted against $D'_{xy}$ (Lilley, 1998). For reference, Appendix A shows a basic Mohr circle with the radius $r$ marked, and extends the diagram to show also an area (another circle) which has the numerical value of the determinant of the 2 × 2 matrix, scaled by $\pi$. The determinant is a further rotational invariant of the matrix.

Figure 3 shows the Mohr diagram for the example matrix [1.75, 1.34; 0.34, 1.25]. Axes are also drawn for $D'_{yx}$ and $D'_{yy}$. The radial arrows from the circle centre to points H and J give eigenvector directions when read as on a dial. (For reading eigenvector directions 'as on a map' see Appendix B.) On Figure 3, eigenvalues are found, and can be read off where the arrowheads touch vertical axes.

In Figure 3, the circle crosses the vertical axes. The two eigenvalues are the intercept values of $D'_{xx}$, where $D'_{yx} = 0$.

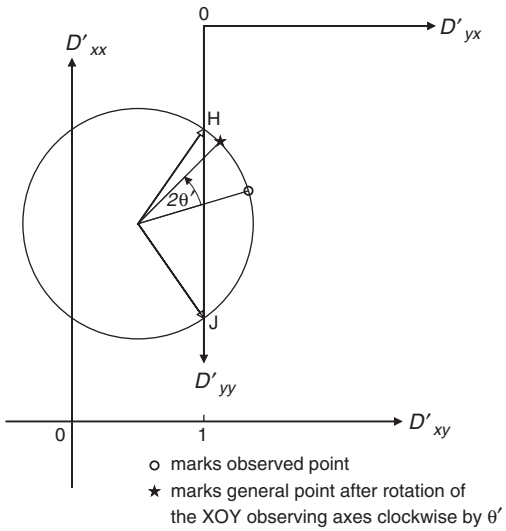


**Fig. 3.** Mohr diagram for eigenanalysis of the example matrix [1.75, 1.34; 0.34, 1.25]. *H* and *J* mark the eigenanalysis positions: the eigenvalues are the $D'_{xx}$ values of points *H* and *J*. The two eigenvector directions are given by the directions of $OX'$ in Figure 1 after a rotation of the observing axes ($XOY$) there causes the radial arm in the present figure to move, respectively, to points *H* and *J*. The unit length scale is marked on the horizontal axis.

Radial arrows are drawn to points H and J, the two $D'_{yx}=0$ intercepts on Figure 3, and the two eigenvector directions are given by the $\theta'$ values for these radial arms. By the symmetry of the figure, the two eigenvalues can be seen to be also given by where the circle intersects the $D'_{xx}$ axis, and are 2.22 and 0.78 in this example.

### *Diagrams for a range of matrices*

Figure 4 shows the Mohr diagram for the example matrix [1.75, 1.34; 0.34, 1.25] in the context of six related matrices. In Figure 4*a*, *b* axes are again drawn for $D'_{yx}$ and $D'_{yy}$.

The three eigenvalue cases just discussed in the section *Formal eigenvalue analysis* are clearly distinguished when the matrices are represented by Mohr diagrams, as in Figure 4. Eigenvalues which are real are shown graphically, and the directions of their eigenvectors are shown as on a dial (not as on a map; though see Appendix B).

The example in Figure 4*a* demonstrates that real eigenvalues correspond to the case of the circle crossing the $D'_{xx}$ and $D'_{yy}$ vertical axes. Further it can be seen that for a Mohr circle to not enclose or capture the origin the product of the two eigenvalues must be positive; i.e. det $\boldsymbol{D}$ must be positive.

Secondly, for the case discussed in the section *Eigenvalues are real and equal*, Figure 4*b* shows a circle which is just touching both the vertical axis $D'_{xy}=0$ and the vertical axis $D'_{yx}=0$. The direction of the repeated eigenvector corresponds to the direction of a radial arm which is horizontal in the diagram, as shown. As for Figure 4*a*, the eigenvalues may be read off the $D'_{xx}$ axis, in this particular case as $(D_{xx}+D_{yy})/2$ (see also Equation 14).

Thirdly, for the case of the section *Eigenvalues are complex conjugate pairs*, circles which (as in Figure 4*c*) do not touch or cross the vertical axes obey Inequality 15. Their eigenvalues are complex conjugate pairs, and real eigenvectors for them do not exist. There is no direction of $\mathbf{E^b}$ for which $\mathbf{E^m}$ is parallel.

Finally it is important to note that the identity matrix [1, 0; 0, 1] shown in Figure 4*e* describes the case of no distortion. Any actual distortion can be viewed as an outgrowth from that identity matrix, and the Mohr diagram for any actual distortion can be viewed as an outgrowth from that single point plotted at $D'_{xx}=1$, $D'_{xy}=0$ (an example will be given in Appendix E).

## SVD

### *Description*

SVD of tensor $\boldsymbol{D}$ produces a rotation for the axes at regional site B, and a (generally) different rotation for the axes at local site M. These rotations are such that a change of electric field along either of the rotated axes at B then produces a change of electric field (generally amplified or attenuated) along the corresponding (differently) rotated axis at M. This situation is depicted in Figure 5.

A regional electric field component in the direction of the regional-site $OX'$ axis will, at the local site, be in the direction of the $OX'$ axis there and, for the matrix used as an example in this paper, be amplified by the singular value 2.46. In Figure 5 the value 2.46 is depicted by the length of the $OX'$ axis at the local site.

Similarly a regional electric field component in the direction of the regional-site $OY'$ axis will, at the local site, be in the direction of the $OY'$ axis there and will be attenuated by the singular value 0.71. The value 0.71 is indicated by the length of the $OY'$ axis at the local site.

### *SVD of a 2 × 2 matrix*

Equations for the SVD of a 2 × 2 matrix may be derived directly. Equation 3 is written as

$$\mathbf{E^m} = \mathbf{R}(-\theta_{\mathrm{m}}).\begin{bmatrix} w_1 & 0 \\ 0 & w_2 \end{bmatrix}.\mathbf{R}(\theta_{\mathbf{b}}).\mathbf{E^b} \tag{21}$$

where the local and regional observation axes are rotated clockwise independently, the local axes by $\theta_m$ and the regional axes by $\theta_b$. Thus the tensor $\boldsymbol{D}$ is factored into

$$\begin{bmatrix} D_{xx} & D_{xy} \\ D_{yx} & D_{yy} \end{bmatrix} = \mathbf{R}(-\theta_{\mathbf{m}}).\begin{bmatrix} w_1 & 0 \\ 0 & w_2 \end{bmatrix}.\mathbf{R}(\theta_{\mathbf{b}}) \tag{22}$$

which may be cast as

$$\begin{bmatrix} w_1 & 0 \\ 0 & w_2 \end{bmatrix} = \mathbf{R}(\theta_{\mathbf{m}}).\begin{bmatrix} D_{xx} & D_{xy} \\ D_{yx} & D_{yy} \end{bmatrix}.\mathbf{R}(-\theta_{\mathbf{b}}) \tag{23}$$

Equation 23, expanded into its four constituent equations, may be solved to give solutions

$$\theta_b + \theta_m = \arctan\left[\frac{D_{xy}+D_{yx}}{D_{xx}-D_{yy}}\right] \tag{24}$$

$$\theta_b - \theta_m = \arctan\left[\frac{D_{xy}-D_{yx}}{D_{xx}+D_{yy}}\right] \tag{25}$$

$$\begin{aligned} w_1 + w_2 = {} & (D_{xy}-D_{yx})\sin(\theta_b-\theta_m) \\ & + (D_{xx}+D_{yy})\cos(\theta_b-\theta_m) \end{aligned} \tag{26}$$

and

$$\begin{aligned} w_1 - w_2 = {} & (D_{xy}+D_{yx})\sin(\theta_b+\theta_m) \\ & + (D_{xx}-D_{yy})\cos(\theta_b+\theta_m) \end{aligned} \tag{27}$$

For the example tensor of Equation 5, the values of $\theta_m$, $\theta_b$, $w_1$ and $w_2$ may be evaluated by the equations above as 27.5°, 45.9°, 2.46 and 0.71 respectively. These are the values shown in Figure 5.

The quantities $w_1$ and $w_2$ are termed singular values (and sometimes principal values, or latent values). An examination of the possibility of a singular value being negative is addressed below.

Should one of the singular values be zero, the matrix itself is then termed ‘singular’. This situation is discussed in several

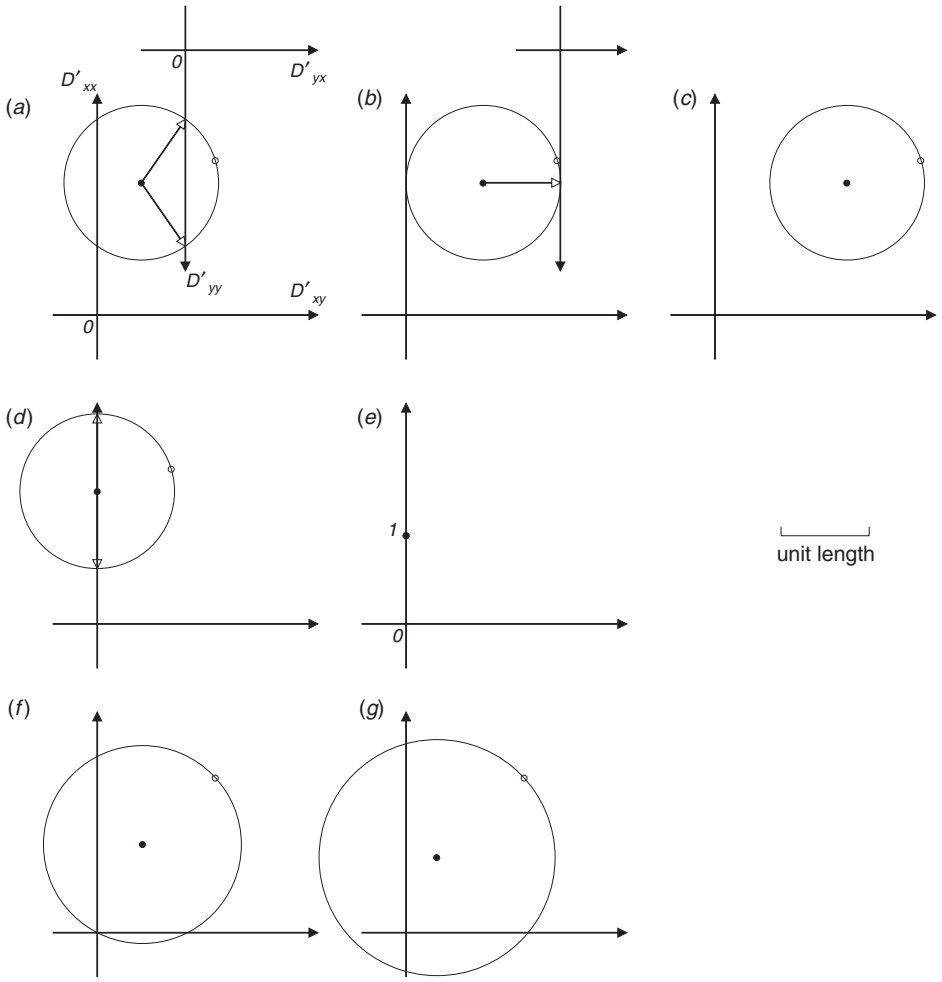


**Fig. 4.** Mohr diagrams for eigenanalysis, using different matrices as examples. (*a*) Matrix [1.75, 1.34; 0.34, 1.25]. Eigenvalues are real and different; eigenvectors are not orthogonal. (*b*) Matrix [1.75, 1.56; −0.04, 1.25]. Eigenvalues are real and equal; both eigenvectors are the same. (*c*) Matrix [1.75, 2.34; −0.66, 1.25]. Eigenvalues are complex conjugates, and are not evident on the diagram. (*d*) Matrix [1.75, 0.84; 0.84, 1.25]. Eigenvalues are real and different; eigenvectors are orthogonal (the 2D case). (*e*) Matrix [1, 0; 0, 1]. The identity matrix, for which both eigenvalues are unity; and all directions are eigenvectors. (*f*) Matrix [1.75, 1.34; 0.33, 0.25]. A matrix which is singular, and has a determinant of zero. (*g*) Matrix [1.75, 1.34; 0.64, −0.05]. A matrix which has a negative determinant, and the Mohr circle encloses the origin. This matrix has one negative and one positive eigenvalue, as can be seen from the intercepts of its circle with the $D'_{xx}$ axis.

places below, especially in the section *A condition number to measure singularity*.

### *Ordering* $w_1 > w_2$

If, following SVD of a $2 \times 2$ matrix, $w_2$ is found to be greater than $w_1$, their order may be changed by remembering that

$$\begin{bmatrix} 0 & -1 \\ 1 & 0 \end{bmatrix} \begin{bmatrix} w_1 & 0 \\ 0 & w_2 \end{bmatrix} \begin{bmatrix} 0 & 1 \\ -1 & 0 \end{bmatrix} = \begin{bmatrix} w_2 & 0 \\ 0 & w_1 \end{bmatrix} \tag{28}$$

and that [0, –1; 1, 0] and [0, 1; –1, 0] both have the form of rotations (see Equation 1).

Solutions found for Equation 22 may therefore be equivalently written

$$\begin{bmatrix} D_{xx} & D_{xy} \\ D_{yx} & D_{yy} \end{bmatrix} = \mathbf{R}(-\theta_m - \pi/2). \begin{bmatrix} w_2 & 0 \\ 0 & w_1 \end{bmatrix} .\mathbf{R}(\theta_b + \pi/2) \tag{29}$$

In Figure 5, increasing $\theta_m$ and $\theta_b$ by $\pi/2$ causes the sets of axes at both sites M and B to be rotated clockwise by 90°, and the significance of the diagram is left unchanged.

### *Changing the sign of a negative singular value*

If $w_2$ is found to be negative, its sign may be changed by remembering

$$\begin{bmatrix} w_1 & 0 \\ 0 & w_2 \end{bmatrix} = \begin{bmatrix} 1 & 0 \\ 0 & -1 \end{bmatrix} \begin{bmatrix} w_1 & 0 \\ 0 & -w_2 \end{bmatrix} \tag{30}$$

so that Equation 22 may be written

$$\begin{bmatrix} D_{xx} & D_{xy} \\ D_{yx} & D_{yy} \end{bmatrix} = \begin{bmatrix} \cos\theta_m & -\sin\theta_m \\ \sin\theta_m & \cos\theta_m \end{bmatrix} \begin{bmatrix} 1 & 0 \\ 0 & -1 \end{bmatrix} \begin{bmatrix} w_1 & 0 \\ 0 & -w_2 \end{bmatrix} .\mathbf{R}(\theta_b) \tag{31}$$

Then, post-multiplying $\mathbf{R}(-\theta_m)$ by [1, 0; 0, –1] gives

$$\begin{bmatrix} D_{xx} & D_{xy} \\ D_{yx} & D_{yy} \end{bmatrix} = \begin{bmatrix} \cos\theta_m & \sin\theta_m \\ \sin\theta_m & -\cos\theta_m \end{bmatrix} \begin{bmatrix} w_1 & 0 \\ 0 & -w_2 \end{bmatrix} .\mathbf{R}(\theta_\mathbf{b}) \tag{32}$$

In Equation 22, the two column vectors $[\cos\theta_m, \sin\theta_m]^\mathbf{T}$ and $[-\sin\theta_m, \cos\theta_m]^\mathbf{T}$ of $\mathbf{R}(-\theta_m)$ give the directions of the axes at site

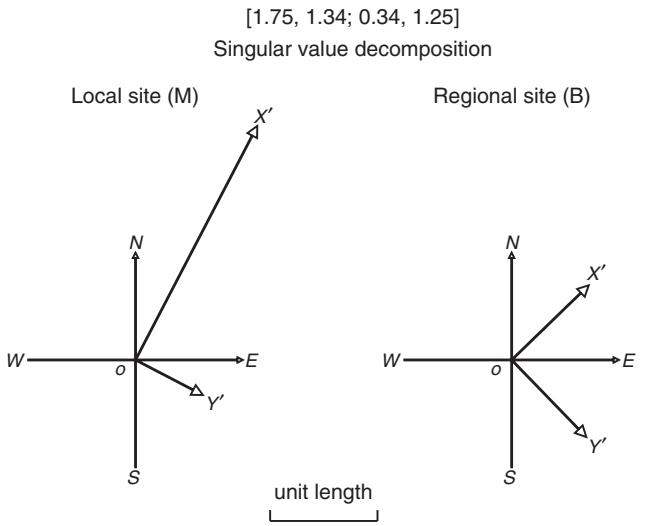


**Fig. 5.** Singular value decomposition. The bearings of the $OX'$ axes are 27.5° (local) and 45.9° (regional). The bearings of the $OY'$ axes are 117.5° (local) and 135.9° (regional).

M in Figure 5. In Equation 32, the first column vector is $[\cos\theta_m, \sin\theta_m]^{\mathbf{T}}$ and unchanged, and so will give an unchanged axis direction. However, the second column vector $[\sin\theta_m, -\cos\theta_m]^{\mathbf{T}}$ has its signs changed, and as a result will give a reversed axis direction. Thus in addition to the rotation of the axes from site B to site M, there has been an axis reflection.

### *Formal SVD*

The results in Figure 5 just described may also be obtained by the formal SVD analysis generally intended for larger matrices. As described for example by Strang (2005), decomposition by SVD factors a matrix $\boldsymbol{D}$ into

$$\boldsymbol{D} = \mathbf{U}.\mathbf{W}.\mathbf{V}^{\mathbf{T}} \tag{33}$$

where $\mathbf{W}$ is diagonal and holds the singular values of $\boldsymbol{D}$. The columns of $\mathbf{V}$ are eigenvectors of $\boldsymbol{D}^{\mathbf{T}}.\boldsymbol{D}$. The columns of $\mathbf{U}$ are eigenvectors of $\boldsymbol{D}.\boldsymbol{D}^{\mathbf{T}}$, and may be found by multiplying $\boldsymbol{D}$ by the columns of $\mathbf{V}$. The singular values on the diagonal of $\mathbf{W}$ are the square roots (taken positive by convention, a most important point in the present context) of the non-zero eigenvalues of $\boldsymbol{D}.\boldsymbol{D}^{\mathbf{T}}$.

### *Use of standard SVD routines*

Standard computing routines (again generally intended for large matrices) are commonly used for SVD, and it may be useful to note that when the matrix of Equation 5 is put into a standard computing routine, the SVD returned is commonly in the form of Equation 33:

$$\boldsymbol{D} = \begin{bmatrix} -.89 & -.46 \\ -.46 & .89 \end{bmatrix} \begin{bmatrix} 2.46 & 0 \\ 0 & .71 \end{bmatrix} \begin{bmatrix} -.70 & -.72 \\ -.72 & .70 \end{bmatrix} \tag{34}$$

which may be given in the form of Equation 22 by expressing it first as

$$\boldsymbol{D} = \begin{bmatrix} .89 & -.46 \\ .46 & .89 \end{bmatrix} \begin{bmatrix} 2.46 & 0 \\ 0 & .71 \end{bmatrix} \begin{bmatrix} .70 & .72 \\ -.72 & .70 \end{bmatrix} \tag{35}$$

then as

$$\boldsymbol{D} = \begin{bmatrix} \cos 27.5^\circ & -\sin 27.5^\circ \\ \sin 27.5^\circ & \cos 27.5^\circ \end{bmatrix} \begin{bmatrix} 2.46 & 0 \\ 0 & .71 \end{bmatrix} \begin{bmatrix} \cos 45.9^\circ & \sin 45.9^\circ \\ -\sin 45.9^\circ & \cos 45.9^\circ \end{bmatrix} \tag{36}$$

and further as

$$\begin{bmatrix} 1.75 & 1.34 \\ 0.34 & 1.25 \end{bmatrix} = \mathbf{R}(-27.5^\circ). \begin{bmatrix} 2.46 & 0 \\ 0 & .71 \end{bmatrix} .\mathbf{R}(45.9^\circ) \tag{37}$$

The columns of the first matrix [cos27.5°, –sin27.5°; sin27.5°, cos27.5°] in Equation 36, which has been derived as $\mathbf{U}$ in Equation 33, define the unit vectors which are drawn for $OX'$ and $OY'$ at the local site in Figure 5. The rows of the third matrix, [cos45.9°, sin45.9°; –sin45.9°, cos45.9°], derived for $\mathbf{V}^{\mathbf{T}}$ in Equation 33, define the unit vectors drawn for $OX'$ and $OY'$ at the regional site in Figure 5. Also, as is evident, the singular values in the diagonal of matrix $\mathbf{W}$ are $w_1$ and $w_2$, the amplifying factors for $E'_x$ and $E'_y$ respectively at the local site. Standard routines will commonly order $w_1 > w_2$.

### *Discussion of SVD results and comparison with eigenanalysis*

By rotation of the local and regional axes separately, the distortion tensor has been reduced by SVD to an ideal 2D form. In a search for the nearest 2D model of distortion in a generally 3D situation the results of SVD may give some insight, but care must be taken in their interpretation. One appealing interpretation worth testing, in the context of known background information, is whether the rotated regional axes give an indication of regional strike, while the rotated local axes give an indication of local 2D strike (to the extent that the concept of a local 2D strike is valid in a 3D situation). For the example matrix analysed above, the SVD result of a unit regional field change at bearing 45.9° giving a local field change of amplitude 2.46 at bearing 27.5°, may be compared with the eigenanalysis result that a unit regional field change at bearing 19.3° gives a local field change of amplitude 2.22 at bearing 19.3°. The discrepancies between the 'best 2D axes' of these results indicates the 3D nature of the matrix analysed, and the hazard of proceeding with 2D modelling in such a case.

### *SVD displayed on a Mohr diagram*

The Mohr diagram for the example matrix in Figures 3 and 4*a* is shown again in Figure 6, where now the results of SVD are displayed. The two singular values $w_1$ and $w_2$ are shown by the intervals $OG$ and $OF$. In Figure 6 the angle by which $OG$ is rotated clockwise from the vertical $D'_{xx}$ axis is $(\theta_b - \theta_m)$, as can be seen from Equation 25. On the circle, to move the observed point anticlockwise by angle $2\theta'$ to $G$ requires a clockwise rotation of the $XOY$ observing axes (as in Figure 1) by angle $\theta' = \theta_m$.

With an extra construction, shown in Appendix C, the Mohr diagram also shows the directions of the SVD axes, as read on a map.

### *Matrix equations displayed by Mohr diagrams, term by term*

Adopting the description of a 2 × 2 matrix by a Mohr diagram, as derived in the section *Eigenvalues on Mohr diagrams*, allows each individual matrix in an equation such as Equation 22 to be illustrated. A complete equation may be represented term by term, as shown for Equation 22 in Figure 7*a*, using the numerical values of Equation 37.

Using these same values of $\theta_m$, $\theta_b$, $w_1$ and $w_2$, Equation 23 may then similarly be depicted, as shown in Figure 7*b*.

## Matrices with negative determinants

In this section, the circumstances and consequences of the matrix having a negative determinant will be addressed.

### *Eigenanalysis*

As is demonstrated in Figure 4*g*, a 2 × 2 matrix with a negative determinant has one positive and one negative eigenvalue. The

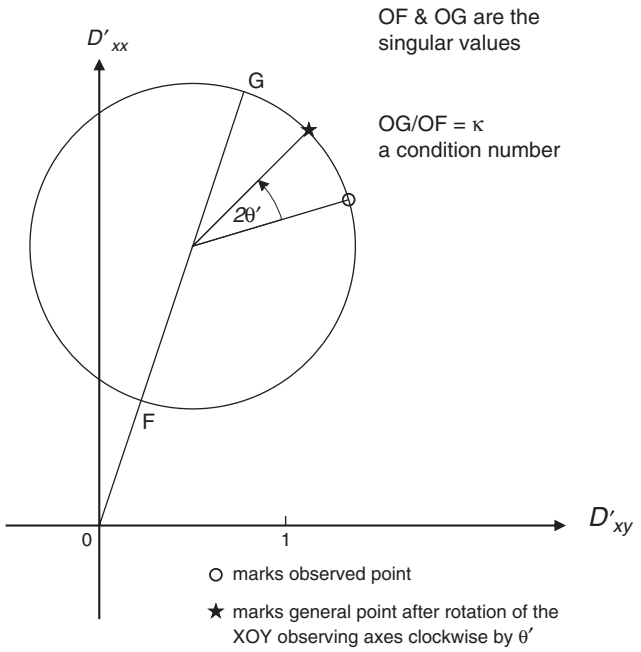


**Fig. 6.** Mohr diagram for singular value decomposition of the example matrix. [1.75, 1.34; 0.34, 1.25]. *OG* and *OF*, 2.46 and 0.71 in length respectively, show the greater and lesser singular values ($w_1$ and $w_2$). The angle *OG* makes with the $D'_{xx}$ axis is $(\theta_b - \theta_m)$. To move the observed point anticlockwise by angle $2\theta_m$ around the circle to point *G* requires a clockwise rotation (as in Figure 1) of the *XOY* observing axes at the local site by angle $\theta_m$. Then, when $2\theta' = 2\theta_m$, the point marked with an asterisk will coincide with point *G*.

eigenvector corresponding to the negative eigenvalue may therefore at the local site be drawn reversed, relative to its direction at the base site. A unit field change in the direction of the eigenvector at the base site will then give a field change at the local site in the direction of the (reversed) eigenvector there, of amplitude equal to the modulus of the negative eigenvalue.

*SVD*

The consequences of a negative determinant for the SVD of a matrix are in some ways more complicated than for the eigenanalysis of the matrix. Following the procedure shown in Figure 5, where axes at site M are simply rotated relative to axes at site B, a matrix with a negative determinant would give a negative singular value for one of the axes.

Following, however, the common convention by which singular values are never quoted negative, it then becomes necessary to reverse the axis at site M for which the singular value has been found to be negative (see the section *Changing the sign of a negative singular value*). By reversing the axis to which it applies, the (otherwise negative) singular value is rendered positive, as required by convention.

## Negative determinants: the situation with distortion matrices, and Groom-Bailey analysis

No case histories of negative determinants for telluric distortion matrices are known to the author, and it is likely that they arise very rarely, if at all. However there are reported cases of magnetotelluric tensors with in-phase and/or quadrature parts with negative determinants, and distortion matrices with negative determinants (should they exist) would be candidates for causing such phenomena.

The Groom-Bailey analysis of the distortion tensor (Groom and Bailey, 1989, 1991), based on their particular decomposition model, is widely used in the analysis of observed magnetotelluric data (Jones, 2012). For reasons which it is instructive to now examine, this decomposition does not cater for the possibility of the distortion matrix having a negative determinant.

Using the notation of Jones (2012) (but with the ***D*** of the present paper) the Groom-Bailey decomposition is

$$\boldsymbol{D} = \mathrm{g}\mathbf{T}.\mathbf{S}.\mathbf{A} \tag{38}$$

where g is a scalar (assumed positive) called site gain. **T**, **S** and **A**, respectively the twist, shear and anisotropy, are expressed

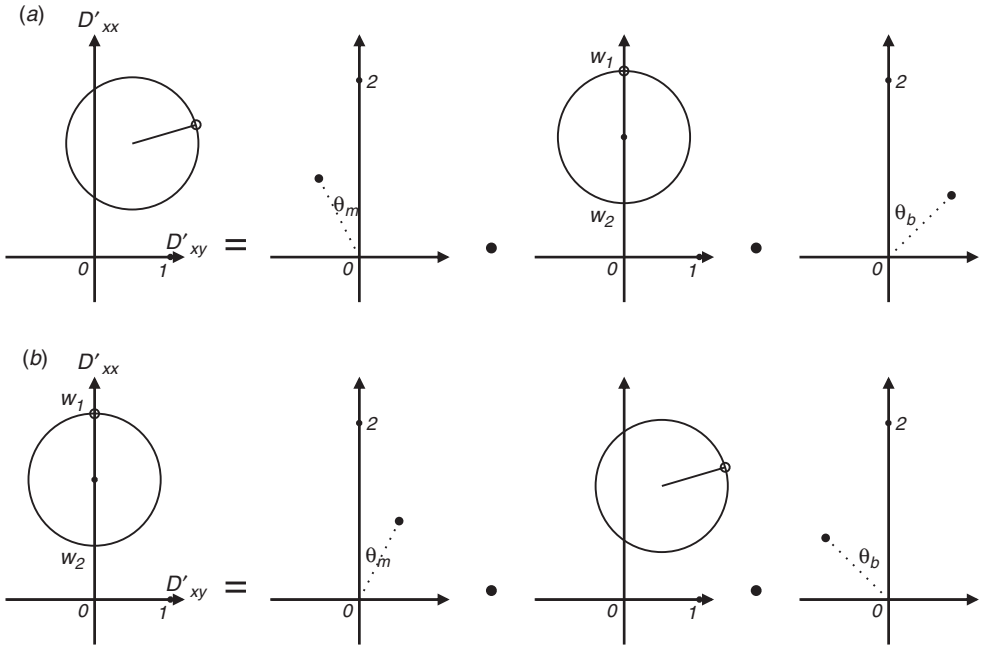


**Fig. 7.** (*a*) Equation 22 shown by Mohr diagrams, term by term, using the values of Equation 37 for the SVD of the example matrix [1.75, 1.34; 0.34,1.25]. (*b*) Equation 23 similarly shown by Mohr diagrams, term by term, for the example matrix [1.75, 1.34; 0.34, 1.25].

$$\mathbf{T} = (1+t^2)^{-1/2}[1, -t; t, 1] \tag{39}$$

$$\mathbf{S} = (1+s^2)^{-1/2}[1, s; s, 1] \tag{40}$$

and

$$\mathbf{A} = (1+a^2)^{-1/2}[1+a, 0; 0, 1-a] \tag{41}$$

in terms, respectively, of scalar quantities $t$, $s$ and $a$. Often 'twist' and 'shear' are expressed as angles, in which case $t$ and $s$, respectively, are the tangent values of those angles. (Note that Equation 39 is comparable to Equation 1 for the definition of axes rotation, but with arctan $t = -\theta$.)

It is useful here to also define a positive factor $f$

$$f = [(1+t^2)(1+s^2)(1+a^2)]^{-1/2} \tag{42}$$

which, when multiplied by the gain g, produces a 'modified gain' $g_m$ :

$$g_m = gf \tag{43}$$

Equation 38 may then be expressed as

$$\boldsymbol{D} = g_m \begin{bmatrix} 1 & -t \\ t & 1 \end{bmatrix} \begin{bmatrix} 1 & s \\ s & 1 \end{bmatrix} \begin{bmatrix} 1+a & 0 \\ 0 & 1-a \end{bmatrix} \tag{44}$$

The determinant of $\boldsymbol{D}$ will be the product of the separate determinants of **T**, **S** and **A**, multiplied by the scalar $g^2$, and may be expressed as

$$\det \boldsymbol{D} = {g_m}^2(1+t^2)(1-s^2)(1-a^2) \tag{45}$$

For $|s| < 1$ and $|a| < 1$, det $\boldsymbol{D}$ will never be negative. Regarding $|s|$, Jones (2012) states that there is a physical limit of unity on $|s|$ in that 'distortion can never be so severe that it will cause the local fields to have a component in the reverse direction to the regional fields'. Regarding $|a|$, Jones (2012) states that 'the obvious physical limit on $|a|$ is that it must be less than unity – an anisotropy $|a| > 1$ would yield negative resistivity in one of the directions'. The value of det D is thus never expected to be negative. While it is certainly not obvious how a local distorting structure could cause a reversal of the telluric electric field, a more comprehensive proof that negative determinants are physically impossible would be a valuable addition to the theory of telluric distortion.

Distortion matrices which are singular, or nearly singular but singular within error, are common and well-known. Jones (2012), for example, when discussing Groom-Bailey shear, notes that the limit on shear angle is 45°, and quotes the case of a narrow valley filled with conducting sediments as exhibiting an electric field in just one direction (a property of a singular distortion matrix). From recognising that singular distortion matrices are not uncommon, it is then a simple step to expect some distortion matrices to be calculated with negative determinants, due simply to experimental error in measurements which, more accurately, would give the zero determinant of the singular case.

A relevant point regarding the Groom-Bailey decomposition is that the anisotropy matrix **A** in Equation 41 has the same form as the SVD matrix in the centre of the right-hand side of Equation 22. In terms of the Groom-Bailey notation, the SVD decomposition of Equation 22 (shown in Figure 7*a*) is $g\mathbf{T_1}.\mathbf{A}.\mathbf{T_2}$, where $\mathbf{T_1}$ and $\mathbf{T_2}$ are different rotations, through angles $-\theta_m$ and $\theta_b$ respectively. For 2D, $\theta_m = \theta_b$.

While in the Groom-Bailey decomposition the only explicit rotation is **T** and it is called 'twist', in SVD (see Equation 22) the term 'twist' is better kept for the difference between the two rotations, $\theta_b$ and $\theta_m$. Twist, defined as $(\theta_b - \theta_m)$, is then zero for 2D. The Groom-Bailey decomposition has the added complication that the shear operator **S** also contributes a rotation.

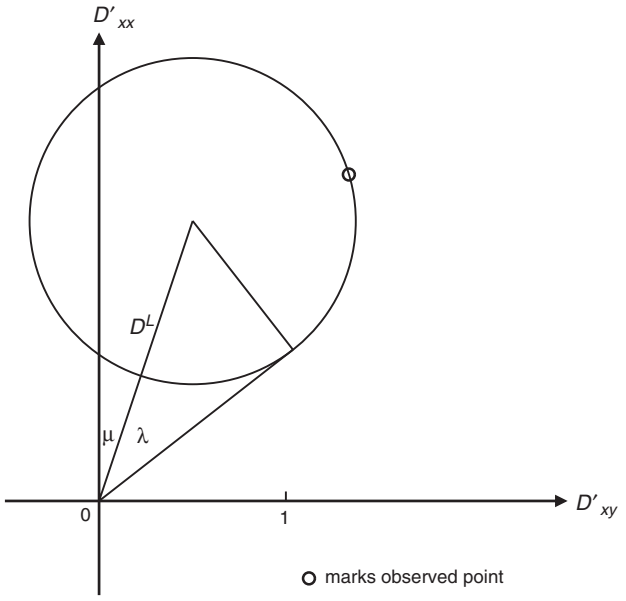


**Fig. 8.** The example matrix [1.75, 1.34; 0.34, 1.25] shown on a Mohr diagram. $D^L$, $\lambda$ and $\mu$ as shown are, by inspection, a straightforward set of invariants which characterise, respectively, the 1D, 2D and 3D properties of the matrix.

In Appendix E below, a comparison of the decompositions $g\mathbf{T}.\mathbf{S}.\mathbf{A}$ and $g\mathbf{T_1}.\mathbf{A}.\mathbf{T_2}$ (the latter returned to the notation of this paper as $\mathbf{R_1}.\mathbf{W}.\mathbf{R_2}$) is made by re-composing each, step by step, in terms of their Mohr diagrams.

## Invariants of rotation in review

Many invariants of rotation of the distortion tensor have been introduced in earlier sections of this paper, and in this section a useful set of invariants which is evident on a Mohr diagram will be summarised.

This set, which the author has found convenient, is shown in Figure 8. Thus $D^L$ gives a gain relative to the undistorted value of unity, $\lambda$ as an angle gives a measure of 2D, and $\mu$ as an angle gives a measure of 3D.

In terms of the quantities in Equation 22, Figures 6 and 8, it can be seen that

$$D^L = (OG + OF)/2 = (w_1 + w_2)/2 \tag{46}$$

$$\begin{aligned} \lambda &= \arcsin[(OG - OF)/(OG + OF)] \\ &= \arcsin[(w_1 - w_2)/(w_1 + w_2)] \end{aligned} \tag{47}$$

and

$$\mu = \theta_b - \theta_m \tag{48}$$

### *A condition number to measure singularity*

It is possible that a distortion tensor will exhibit very strong anisotropy and, as a consequence, the tensor will approach a condition of singularity. In a Mohr diagram the condition of singularity is shown by a circle touching the origin, as in Figure 4*f*. If, for example, $\boldsymbol{D}$ is a singular tensor, then there is some rotation of axes for which both $D'_{xx}$ and $D'_{xy}$ are zero (or indistinguishable from zero, when error is taken into account). For the student of linear algebra, an example of a null space occurs: it is the line of the direction of regional electric field change which causes nil

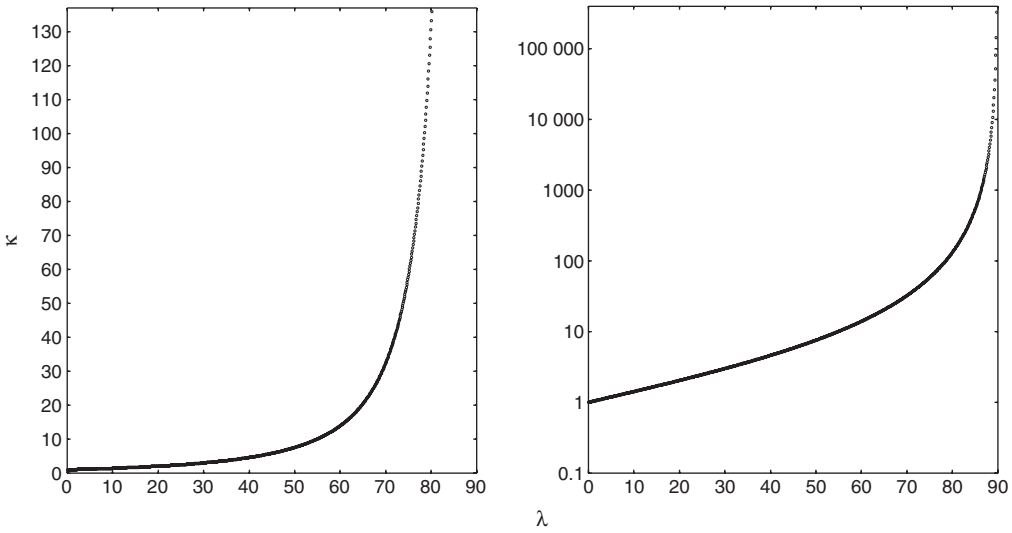


**Fig. 9.** The condition number $\kappa$ displayed as a function of the anisotropy angle $\lambda$ in degrees, using linear (left) and logarithmic (right) scales for $\kappa$.

local electric field change. An example of this null space is discussed in Appendix D, taking the singular matrix given in Figure 4*f*.

A condition number may be used to warn that singularity is being approached (Strang, 2005). When the condition number becomes high in some sense, the matrix is said to be ill-conditioned (Press et al., 1989). The condition number suggested by Strang (2005) is the norm of the matrix (sometimes called the spectral norm) multiplied by the norm of the inverse of the matrix; or equivalently, the greater principal value of the matrix divided by the lesser principal value. For the $2 \times 2$ matrix $\boldsymbol{D}$ in Equation 22 the condition number $\kappa$ is

$$\kappa = w_1/|w_2| \tag{49}$$

where the greater and lesser principal values $w_1$ and $w_2$ (given by Equations 26 and 27 above) are the singular values of the matrix. Following the convention that singular values are never negative, a modulus sign is put into the denominator of Equation 49 to cover cases where the lesser principal value might otherwise be determined as negative using Equations 26 and 27. In terms of the Mohr representations in Figure 6, from Equation 49 the condition number is given by

$$\kappa = OG/OF \tag{50}$$

that is,

$$\kappa = 1 + 2/(\mathrm{cosec}\lambda - 1) \tag{51}$$

with $\lambda$ defined as in Figure 8 and Equation 47. Figure 9 shows $\kappa$ as a function of $\lambda$. While $\lambda$ itself is a measure of condition, Figure 9 demonstrates that $\kappa$ is more sensitive than $\lambda$ as ill-condition is approached. Note that $\kappa \geq 1$, for all $\lambda$.

### *An anisotropy number*

The complication, caused by a negative determinant in the definition of the condition number, suggests that in place of the latter a number might be useful which is defined as the ratio of the radius of the Mohr circle ($r$ in Equation 20) to the distance of the centre of the circle from the origin ($D^L$ in Figure 8). Denoting such an 'anisotropy number' by $A$, then (for $w_1$ ordered greater than $w_2$; see the section *Ordering* $w_1 > w_2$),

$$A = r/D^L = (w_1 - w_2)/(w_1 + w_2) \tag{52}$$

Such an anisotropy number will be less than unity for positive determinants; be unity for singular matrices; and be greater than unity for determinants which are negative. There will then be no need for concern with conventions such as that under which singular values are always quoted positive.

It can be seen from Equation 47 that for $A \leq 1$, $\lambda$ and $A$ are linked by

$$\lambda = \arcsin A \tag{53}$$

## Some further examples

In this section, three distortion matrices, already well-studied, will be analysed by eigenanalysis and SVD as further examples of the application of these techniques. The examples are from different origins but all are described by Jones (2012), to whose discussion it is strongly recommended the reader refer. For these examples, Jones (2012) gives values for the Groom-Bailey decomposition parameters of twist, shear, anisotropy and gain, which will be quoted here for comparison. However, it is the experience of the present author that while the terms 'twist' and 'shear' have their origin in practical matters which can be visualised, in fact as they occur in the Groom-Bailey analysis their visualisation is not straightforward. Thus they are not clearly evident on a Mohr diagram for a distortion tensor, which otherwise shows a wide range of invariants.

### *Larsen and Hawaii*

The first case comes from Larsen (1975) as presented by Jones (2012) in the form of Equation 3. The distortion matrix is quoted as [0.803, 0.835; 0.635, 1.197]. Jones (2012) describes this example as being one of relatively strong distortion, with values of 1.7°, 36.6°, 0.175 and 0.996 for the Groom-Bailey parameters of twist, shear, anisotropy and gain respectively.

#### *Eigenanalysis*

Eigenanalysis as described above gives eigenvectors of magnitudes 1.75 and 0.25 at bearings 48.5° and –33.4° respectively. These eigenanalysis results are presented in map form on the left-hand side of Figure 10.

#### *SVD*

SVD as described above gives axes rotations of –34.7° and –40.4° for the regional and local sites respectively, with

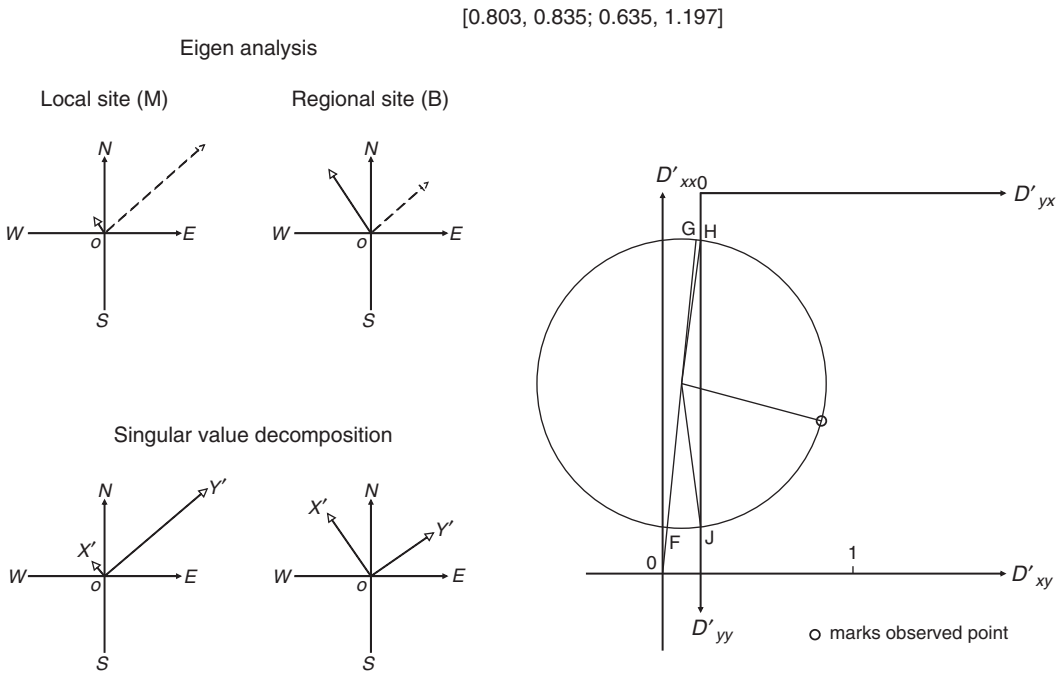


**Fig. 10.** Eigenanalysis, SVD and Mohr diagram for the Larsen matrix.

amplifications of 0.25 and 1.77 in the $OX'$ and $OY'$ directions at the local site. These SVD results are also presented in map form on the left-hand side of Figure 10. A comparison of the eigenanalyses and SVD results shows them to be very similar, indicating that the matrix is close to 2D.

### *Mohr diagram*

The eigenanalysis and SVD results are also shown in the Mohr diagram for the matrix, as displayed in Figure 10.

From the Mohr diagram, the distortion can be seen to be strongly 2D. In terms of the invariants shown in Figure 8 to characterise dimensionality, the values in Figure 10 are $D^L = 1.0$, $\lambda = 49.1°$, and $\mu = 5.7°$. This small value of $\mu$ (the indicator of 3D structure) may be barely distinguishable from zero, when likely error is taken into account.

### *Model computation of Groom and Bailey*

The next example comes from the response computed for a simple model by Groom and Bailey (1991). The distortion matrix is

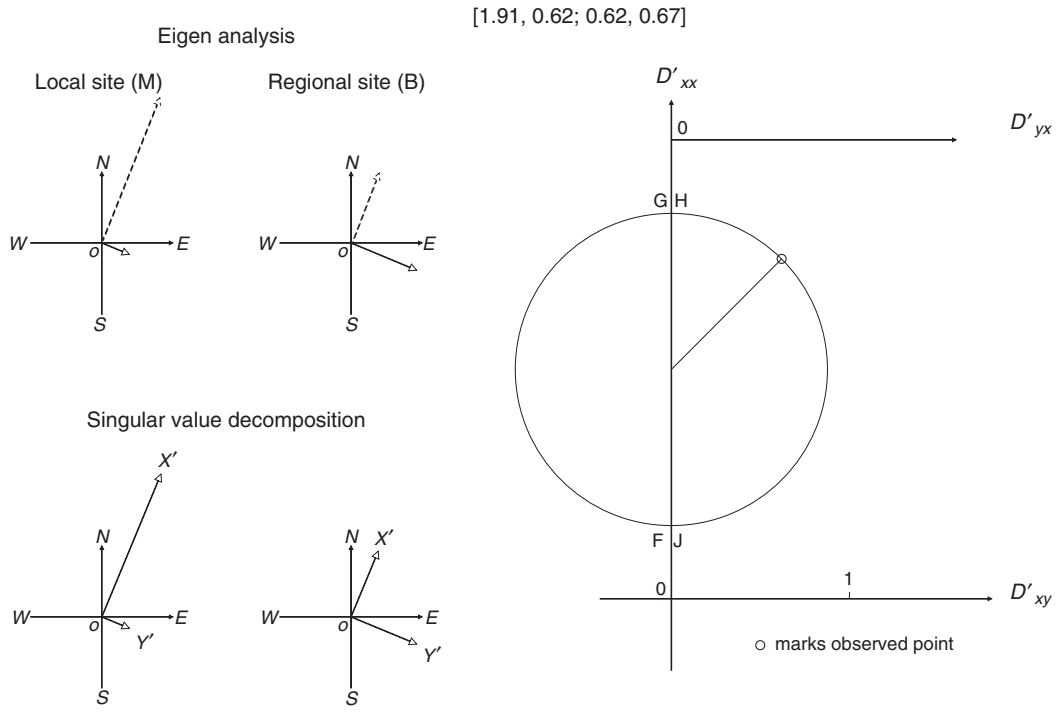


**Fig. 11.** The Groom-Bailey matrix. The geographic axes for the 'local site' and 'regional site' figures are those relative to which the distortion matrix is quoted, and may not be north and east.

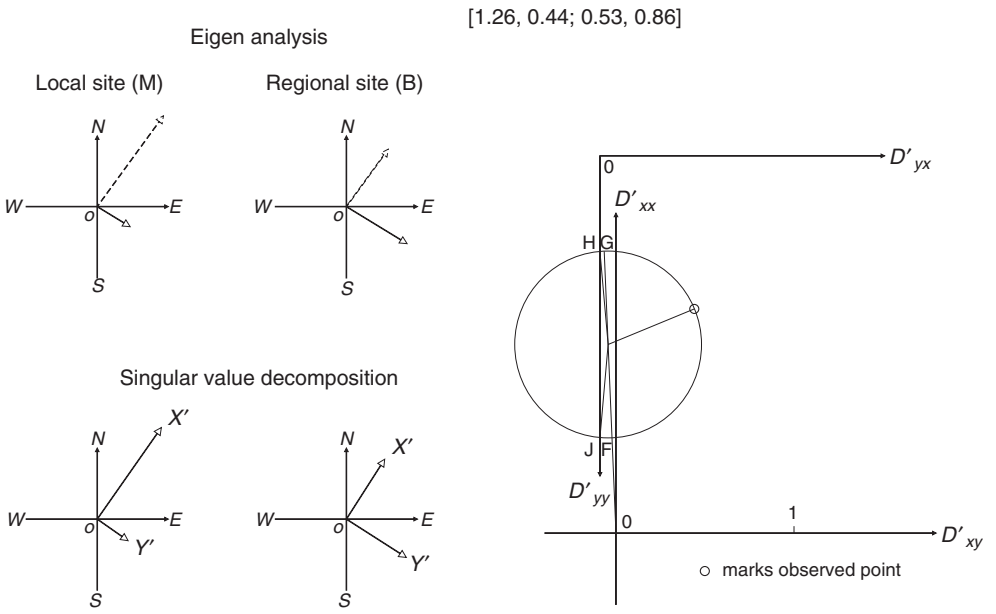


**Fig. 12.** Eigenanalysis, SVD and Mohr diagram for the Chakridi matrix.

quoted as [1.91, 0.62; 0.62, 0.67]. Jones (2012) describes this example as being one of moderate distortion, with values of –12.2°, 30.2°, 0.37 and 1.23 for the Groom-Bailey parameters of twist, shear, anisotropy and (modified) gain respectively. The matrix is immediately seen to be symmetric, and so will have the 2D characteristics evident in Figure 4*d*.

### *Eigenanalysis*

Eigenanalysis as described above gives eigenvectors of magnitudes 2.16 and 0.42 at bearings 21.8° and –67.4° respectively. These eigenanalysis results, with the eigenvector of bearing -67.4° given its reverse direction of 112.6° for easier comparison with the SVD results, are presented in map form on the left-hand side of Figure 11.

### *SVD*

SVD as described above gives axes rotations of 22.5° and 22.5° for the regional and local sites respectively, with amplifications of 2.17 and 0.42 in the $OX'$ and $OY'$ directions at the local site. These SVD results are also presented in map form on the left-hand side of Figure 11.

This SVD result of 22.5° is consistent with the geometry of the model considered by Groom and Bailey (1991). Following Jones, adding the twist (–12.2°) and shear (30.2°) values gives 18.0° for the 'current channelling azimuth', which is close to, but perhaps significantly discrepant from, the 22.5° SVD result (and the model geometry).

### *Mohr diagram*

The eigenanalysis and SVD results are also shown in the Mohr diagram for the matrix, as displayed in Figure 11.

From the Mohr diagram, the distortion can be seen to be purely 2D. In terms of the invariants shown in Figure 8 to characterise dimensionality, the values in Figure 11 are $D^L = 1.3$, $\lambda = 42.7°$, and $\mu = 0.0°$.

This matrix example is discussed further in Appendix E. There, its Groom-Bailey and singular value decompositions are compared, by using them to 're-compose' the matrix, step by step.

### *Chakridi case*

This example also comes from the response computed for a simple model, in this case by Chakridi et al. (1992). The matrix is quoted as [1.26, 0.44; 0.53, 0.86].

Jones (2012) describes this matrix as also being one of moderate distortion, with values of –2.1°, 25.0°, 0.17 and 1.06 for the Groom-Bailey parameters of twist, shear, anisotropy and (modified) gain respectively.

### *Eigenanalysis*

Eigenanalysis as described above gives eigenvectors of magnitudes 1.58 and 0.54 at bearings 36.1° and –58.6° respectively. These eigenanalysis results, with the eigenvector of bearing -58.6° given its reverse direction of 121.4° for easier comparison with the SVD results, are presented in map form on the left-hand side of Figure 12.

### *SVD*

SVD as described above gives axes rotations of 35.0° and 32.6° for the regional and local sites respectively, with amplifications of 1.57 and 0.53 in the $OX'$ and $OY'$ directions at the local site. These SVD results are also presented in map form on the left-hand side of Figure 12.

A comparison of the eigenanalyses and SVD results shows them to be very similar, indicating that the matrix is close to 2D.

### *Mohr diagram*

The eigenanalysis and SVD results are also shown in the Mohr diagram for the matrix, as displayed in Figure 12.

From Figure 12, the distortion can be seen to be strongly 2D, with 3D characteristics barely distinguishable above likely error level. In terms of the invariants shown in Figure 8 to characterise dimensionality, the values in Figure 12 are $D^L = 1.0$, $\lambda = 30.0°$, and $\mu = -2.4°$. This small value of $\mu$ (the indicator of 3D structure) may be barely detectable as different from zero, when error is taken into account.

## Conclusions

The 2 × 2 matrix which describes the local distortion of the electric field in natural electromagnetic induction in the Earth provides

practical examples with which to demonstrate the processes of eigenanalysis and SVD. Distortion matrices which approach singularity arise from time to time, and because they are incorporated as multipliers in both the in-phase and quadrature parts of observed magnetotelluric impedance tensors, they may disrupt the analysis of magnetotelluric data. Monitoring any approach to singularity with a condition number may therefore be useful. An anisotropy number as introduced may also be useful, and has the advantage of showing clearly when a matrix has a negative determinant.

A Mohr diagram for a 2 × 2 matrix is shown to be versatile in displaying a wide range of the properties of the matrix, especially those which are invariant with rotation of the reference axes. Several of the quantities depicted in a Mohr diagram may be useful as measures of the extent to which the matrix is diagnostic of 1D, 2D or 3D geological structure.

## Acknowledgements

The author thanks Peter Milligan, Chris Phillips and John Weaver, who have contributed many ideas and much discussion to the material presented in this paper. Chris Phillips is especially thanked for suggesting many improvements to the presentation of the manuscript. Similarly comments by the associate editor and two reviewers have been very valuable and are much appreciated.

## References

Chakridi, R., Chouteau, M., and Mareschal, M., 1992, A simple technique for analyzing and partly removing galvanic distortion from the magnetotelluric impedance tensor: application to Abitibi and Kapuskasing data (Canada): *Geophysical Journal International*, **108**, 917–929.

Eggers, D. E., 1982, An eigenstate formulation of the magnetotelluric impedance tensor: *Geophysics*, **47**, 1204–1214.

Groom, R. W., and Bailey, R. C., 1989, Decomposition of magnetotelluric impedance tensors in the presence of local three-dimensional galvanic distortion: *Journal of Geophysical Research*, **94**, 1913–1925.

Groom, R. W., and Bailey, R. C., 1991, Analytical investigations of the effects of near surface three dimensional galvanic scatterers on MT tensor decomposition: *Geophysics*, **56**, 496–518.

Jones, A. G., 2012, Distortion of magnetotelluric data: its identification and removal, *in* A. D. Chave, and A. G. Jones, eds., *The magnetotelluric method: theory and practice*: Cambridge University Press, 219–302.

Korner, T. W., 1990, *Fourier analysis*: Cambridge University Press.

Larsen, J. C., 1975, Low-frequency (0.1-6.0 cpd) electromagnetic study of deep mantle electrical-conductivity beneath Hawaiian islands: *Geophysical Journal of the Royal Astronomical Society*, **43**, 17–46.

LaTorraca, G. A., Madden, T. R., and Korringa, J., 1986, An analysis of the magnetotelluric impedance for three-dimensional conductivity structures: *Geophysics*, **51**, 1819–1829.

Lilley, F. E. M., 1993, Magnetotelluric analysis using Mohr circles: *Geophysics*, **58**, 1498–1506.

Lilley, F. E. M., 1998, Magnetotelluric tensor decomposition: Part I, Theory for a basic procedure: *Geophysics*, **63**, 1885–1897.

Lilley, F. E. M., 2012, Magnetotelluric tensor decomposition: insights from linear algebra and Mohr diagrams, *in* H. S. Lim, ed., *New achievements in geoscience*: InTech Open Science, chap. 4, 81–106.

Press, W. H., Teukolsky, S. A., Vetterling, W. T., and Flannery, B. P., 1989, *Numerical recipes: the art of scientific computing*: Cambridge University Press.

Strang, G., 2005, *Linear algebra and its applications* (4th edition): Brooks–Cole.

Telford, W. M., Geldart, L. P., Sheriff, R. E., and Keys, D. A., 1976, *Applied geophysics*: Cambridge University Press.

Weidelt, P., and Chave, A. D., 2012, The magnetotelluric response function, *in* A. D. Chave, and A. G. Jones, eds., *The magnetotelluric method: theory and practice*: Cambridge University Press, 122–164.

Yee, E., and Paulson, K. V., 1987, The canonical decomposition and its relationship to other forms of magnetotelluric impedance tensor analysis: *Journal of Geophysics*, **61**, 173–189.

## Appendix A
## Basic Mohr diagram and value of determinant

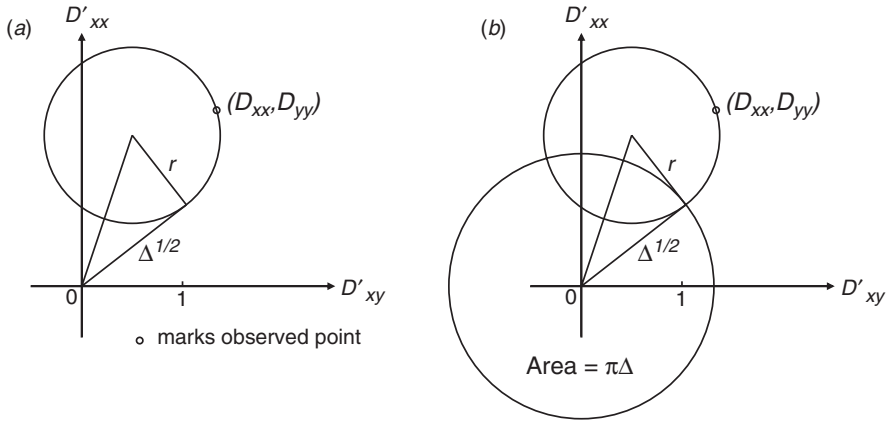


**Fig. A-1.** (*a*) A Mohr diagram for a 2 × 2 matrix showing the observed point ($D_{xx}$, $D_{xy}$), the circle of radius *r*, and the tangent to the circle from the origin, which is of length $\Delta^{1/2}$. (*b*) A second circle, with centre at the origin, has been added to (*a*). This second circle has an area of $\pi\Delta$, where $\Delta$ is the numerical value of the determinant of the matrix, and must be positive for this diagram to apply.

For reference, a basic Mohr diagram with circle radius *r* is shown in Figure A-1*a*. Application of Pythagoras' theorem shows that the tangent is of length equal to the square root of the determinant ($\Delta$) of the matrix. The determinant is also an invariant with the rotation of axes.

There is often interest in displaying the numerical value of the determinant of a 2 × 2 matrix, when that value is positive (Korner, 1990). On a Mohr diagram it is possible to display the numerical value of $\Delta$ in several ways. One way is simply to complete a square, based on the tangent which is shown in Figure A-1*a* to be of length $\Delta^{1/2}$. Another way is shown in Figure A-1*b*, where the circle centred on the origin has an area of $\pi\Delta$.

## Appendix B
## Construction on a Mohr diagram to show eigenvector directions read as on a map

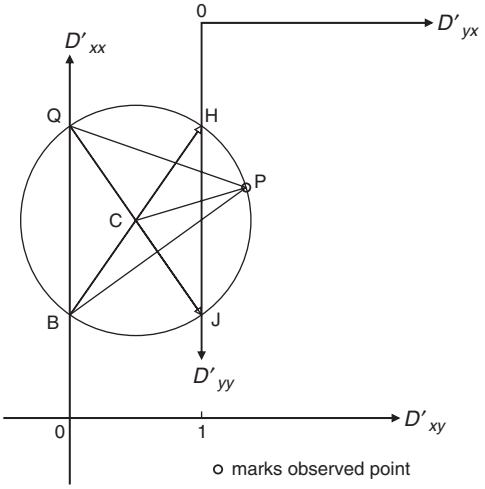


**Fig. B-1.** Matrix [1.75, 1.34; 0.34, 1.25]. Figure 3 reproduced with some deletions for simplification, and with constructions which now give the directions of the eigenvectors, as read on a map (see text).

Figure 3 is reproduced as Figure B-1 with some deletions for simplification, and with constructions which give the directions of the eigenvectors, as read on a map.

As described in the section *Eigenvalues on Mohr diagrams* and Figure 3, directions *CH* and *CJ* in Figure B-1 give the eigenvector directions, reading Figure B-1 as a dial. Rotating the observing axes clockwise in Figure 1 by ½∠*HCP* moves *P* to *H* in Figure B-1, and *OX′* in Figure 1 is then aligned with the eigenvector.

Because ∠*HBP* = ½∠*HCP*, the direction on Figure B-1 of *BP* gives the direction (as on a map) of the eigenvector, relative to *BH* taken as north and the initial axes left unrotated.

For the second eigenvector, represented by direction *CJ*, similar reasoning leads to its direction on a map being shown by line *QP*, when *QJ* is aligned north. (It will be remembered that an eigenvector can with equal validity be drawn either 'forward' or 'reversed'.)

## Appendix C
## Construction on a Mohr diagram to show SVD directions read as on a map

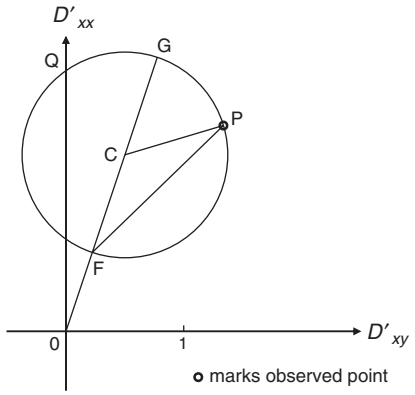


**Fig. C-1.** Matrix [1.75, 1.34; 0.34, 1.25]. Figure 6 reproduced with some deletions for simplification, and with constructions which now give the directions of the SVD axes as read on a map (see text).

Figure 6 is reproduced as Figure C-1 with some deletions for simplification, and with constructions which give the directions of the SVD axes, as read on a map.

In Figure C-1, ∠*GCP* = $2\theta_m$, so ∠*GFP* = $\theta_m$. Because ∠*QOG* = ($\theta_b - \theta_m$), when *OQ* is directed north the line *FP* is at bearing $\theta_b$, and thus shows the bearing of the *OX′* axis at the regional site. Further, if *OG* instead is directed to the north, *FP* is then at bearing $\theta_m$, and shows the direction of the *OX′* axis at the local site.

## Appendix D
## A practical example of a null space

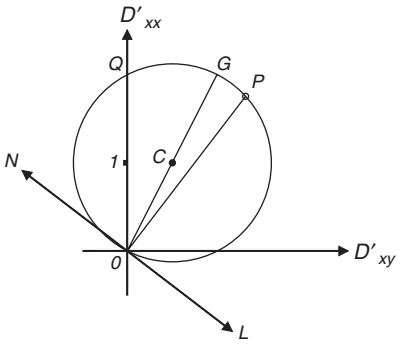


**Fig. D-1.** The singular matrix [1.75, 1.34; 0.33, 0.25] from Figure 4*f* with constructions which show that the null space of the matrix is the line *NL*. In construction, line *NL* is perpendicular to the line joining the observed point *P* to the $D'_{xx}$, $D'_{xy}$ origin.

Matrix [1.75, 1.34; 0.33, 0.25] from Figure 4*f* is singular because its two rows, [1.75, 1.34] and [0.33, 0.25], are not independent. The former is 5.3 times the latter.

Following for example Strang (2005), the null space of the $\boldsymbol{D}$ of Equation 3 consists of all solutions $\mathbf{E^b}$ which satisfy

$$\boldsymbol{D}.\mathbf{E^b} = 0 \tag{D-1}$$

Rotation of the axes as in Figure 1 for matrix [1.75, 1.34; 0.33, 0.25], so that the observed point in Figure 4*f* moves to the $D'_{xx}$, $D'_{xy}$ origin, will render both $D'_{xx}$ and $D'_{xy}$ zero. Equation D-1 then becomes

$$\begin{bmatrix} 0 & 0 \\ D'_{yx} & D'_{yy} \end{bmatrix} \begin{bmatrix} E_x^{b\prime} \\ E_y^{b\prime} \end{bmatrix} = 0 \tag{D-2}$$

The solution of this equation is

$$D'_{yx}E_x^{b\prime} + D'_{yy}E_y^{b\prime} = 0 \tag{D-3}$$

which is satisfied for all field changes which obey

$$E_y^{b\prime}/E_x^{b\prime} = -D'_{yx}/D'_{yy} \tag{D-4}$$

Field changes of components ($E_x^{b\prime}$, $E_y^{b\prime}$) have direction arctan($E_y^{b\prime}/E_x^{b\prime}$), relative to the now rotated axes. Thus the line at bearing arctan($-D'_{yx}/D'_{yy}$) (again relative to the now rotated axes) defines the line of the null space of $\boldsymbol{D}$.

Taking the matrix [1.75, 1.34; 0.33, 0.25] as a numerical example, Equation D-1 becomes

$$\begin{bmatrix} 1.75 & 1.34 \\ 0.33 & 0.25 \end{bmatrix} \begin{bmatrix} E_x^b \\ E_y^b \end{bmatrix} = 0 \tag{D-5}$$

which, solved directly, is found to be satisfied by an $E_y^b/E_x^b$ ratio of –1.3. The value of arctan(–1.30) is –53° or 127°, and so the line of null space has bearing (relative to the original geographic axes) of 127°. This result means that any electric field change at the base site B with bearing 127° will cause nil electric field change at the measurement site M.

Following Appendix C, the direction of the null line on a map is shown on the Mohr diagram. Figure D-1 is Figure 4*f* redrawn and augmented. With reference to Figure D-1, $\angle QOG = (\theta_b - \theta_m)$ and, because $\angle GCP = 2\theta_m$, $\angle GOP = \theta_m$. Therefore $\angle QOP = \theta_b$, and for alignment with the SVD axes of the matrix as in Figure 5, at site B the axes should be rotated clockwise through this angle. Thus for *OQ* aligned north as on a map, *OP* is then the direction of the *OX′* axis at site B. Because the axes in Figure 5 are orthogonal, it follows that $(\theta_b + \pi/2)$ is the direction of signal at site B which will produce nil signal at site M. In Figure D-1 line *NL*, drawn perpendicular to *OP*, has this $(\theta_b + \pi/2)$ direction.

As a check, $\theta_b$ for this matrix may be found from Equations 24 and 25 to be 37°. On Figure D-1, relative to *OQ* as north, line *NL* is at bearing 127°; i.e. at bearing $(\theta_b + \pi/2)$.

## Appendix E
## Two re-compositions compared

The example presented in the section *Model computation of Groom and Bailey* is illustrated here in greater detail. Each step in the multiplication involved in the Groom-Bailey decomposition is presented, as a re-composition, in a series of Mohr diagrams on the left-hand side of Figure E-1. For comparison, on the right-hand side of Figure E-1 the SVD of the same matrix is presented as a re-composition.

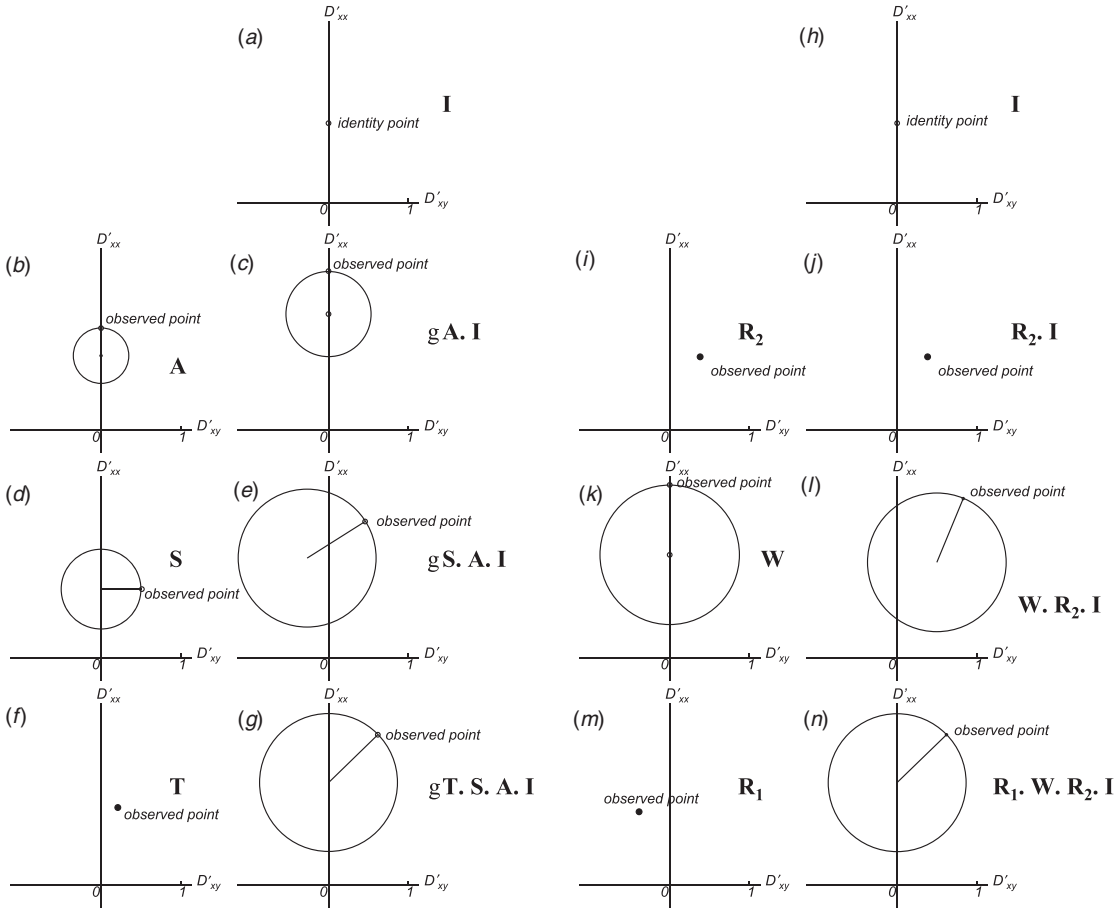


**Fig. E-1.** (*a–g*) Re-composition of the Groom-Bailey matrix, in steps down the figure (see text). (*h–n*) The equivalent SVD re-composition, in steps down the figure (see text).

Thus, on the left-hand side of Figure E-1:

Part (*a*) shows the identity matrix, representing the case of no distortion.
Part (*b*) shows the matrix **A**.
Part (*c*) shows the result of g**A** acting on the identity matrix to give g**A**.**I**, where the scalar gain factor g (of value 1.55) has also been incorporated in this step.
Part (*d*) shows the matrix **S**.
Part (*e*) shows the result of **S** acting on g**A**.**I**, to give g**S**.**A**.**I**.
Part (*f*) shows the matrix **T**.
Part (*g*) shows **T** acting on g**S**.**A**.**I** to give, as g**T**.**S**.**A**.**I**, the matrix ***D*** and, indeed, the Mohr diagram shown in Figure 11.

For comparison, on the right-hand side of Figure E-1:

Part (*h*) again first shows the identity matrix, representing the case of no distortion.
Part (*i*) shows the matrix $\mathbf{R_2}$.
Part (*j*) shows the result of $\mathbf{R_2}$ acting on the identity matrix, to give $\mathbf{R_2}$.**I**.
Part (*k*) shows the matrix **W**.
Part (*l*) shows the result of **W** acting on $\mathbf{R_2}$.**I**, to give **W**.$\mathbf{R_2}$.**I**.
Part (*m*) shows the matrix $\mathbf{R_1}$.
Part (*n*) shows $\mathbf{R_1}$ acting on **W**.$\mathbf{R_2}$.**I** to give, as $\mathbf{R_1}$.**W**.$\mathbf{R_2}$.**I** the matrix ***D*** and, again, the Mohr diagram shown in Figure 11.

An important point to note is that Groom-Bailey decomposition allocates 2D characteristics by both **A** and **S**, the latter of which also contributes a 3D rotation. In contrast, the SVD treatment shows a sole 2D component (**W** in Figure E-1) and 3D contributions enter as rotations only.